Toxicology 269 (2010) 136–147

Contents lists available at ScienceDirect

Toxicology

journal homepage: www.elsevier.com/locate/toxicol

Mouse pulmonary dose- and time course-responses induced by exposure to multi-walled carbon nanotubes

Dale W. Porter[a,b,*], Ann F. Hubbs[a], Robert R. Mercer[a,b], Nianqiang Wu[c], Michael G. Wolfarth[a], Krishnan Sriram[a], Stephen Leonard[a], Lori Battelli[a], Diane Schwegler-Berry[a], Sherry Friend[a], Michael Andrew[a], Bean T. Chen[a], Shuji Tsuruoka[d], Morinobu Endo[d], Vincent Castranova[a,b]

[a] National Institute for Occupational Safety and Health, Morgantown, WV 26505, USA
[b] West Virginia University, Department of Physiology and Pharmacology, Morgantown, WV 26506, USA
[c] West Virginia University, Department of Mechanical & Aerospace Engineering, Morgantown, WV 26506, USA
[d] Shinshu University, Faculty of Engineering, Nagano, Japan

ARTICLE INFO

Article history:
Received 9 May 2009
Received in revised form 2 September 2009
Accepted 15 October 2009
Available online 24 October 2009

Keywords:
Multi-walled carbon nanotubes
Inflammation
Fibrosis

ABSTRACT

Carbon nanotubes (CNT) come in a variety of types, but one of the most common forms is multi-walled carbon nanotubes (MWCNT). MWCNT have potential applications in many diverse commercial processes, and thus human exposures are considered to be likely. In order to investigate the pulmonary toxicity of MWCNT, we conducted an in vivo dose-response and time course study of MWCNT in mice in order to assess their ability to induce pulmonary inflammation, damage, and fibrosis using doses that approximate estimated human occupational exposures. MWCNT were dispersed in dispersion medium (DM) and male C57BL/6J mice (7 weeks old) received either DM (vehicle control), 10, 20, 40 or 80 μg MWCNT by aspiration exposure. At 1, 7, 28 and 56 days post-exposure, MWCNT-induced pulmonary toxicity was investigated. Bronchoalveolar lavage (BAL) studies determined pulmonary inflammation and damage was dose-dependent and peaked at 7 days post-exposure. By 56 days post-exposure, pulmonary inflammation and damage markers were returning to control levels, except for the 40 μg MWCNT dose, which was still significantly higher than vehicle control. Histopathological studies determined that MWCNT exposure caused rapid development of pulmonary fibrosis by 7 days post-exposure, that granulomatous inflammation persisted throughout the 56-day post-exposure period, and also demonstrated that MWCNT can reach the pleura after pulmonary exposure. In summary, the data reported here indicate that MWCNT exposure rapidly produces significant adverse health outcomes in the lung. Furthermore, the observation that MWCNT reach the pleura after aspiration exposure indicates that more extensive investigations are needed to fully assess if pleural penetration results in any adverse health outcomes.
Published by Elsevier Ireland Ltd.

1. Introduction

The development of synthetic carbon nanotubes comprised of cylindrically arranged graphite sheets with a nanoscale diameter permitted rapid advances in nanotechnology. The number of carbon layers in the nanotubes varies from one layer in the single-walled carbon nanotubes (SWCNT) to many layers in the multi-walled carbon nanotubes (MWCNT). Carbon nanotubes (CNT) have potential applications in medical devices, electronic devices, supercapacitors, batteries, the automotive industry, aerospace industry and other important commercial processes (Endo et al., 2008; Tenne et al., 2008).

The potential for occupational exposures to carbon nanotubes is, therefore, increasing but very little is currently known about these exposures. One study reports peak airborne levels of respirable SWCNT particles up to 53 $\mu g/m^3$ (Maynard et al., 2004). A more recent study reports MWCNT-containing airborne dust levels from undetectable to approximately 400 $\mu g/m^3$ in a research laboratory, although the total mass concentration reported in this study was not comprised exclusively of MWCNT (Han et al., 2008). Nonetheless, these studies established that inhalation exposure to airborne CNT is of major occupational concern.

Although CNT come in a variety of types, SWCNT and MWCNT are currently the predominant forms being studied. The acute lung toxicity of intratracheally (IT) instilled SWCNT has been evaluated in rats (Warheit et al., 2004). This study reported that exposure to SWCNT produced transient inflammation and a

* Corresponding author at: Pathology and Physiology Research Branch, Health Effects Laboratory Division, National Institute for Occupational Safety and Health, 1095 Willowdale Road, M/S 2015, Morgantown, WV 26505, USA.
Tel.: +1 304 285 6320; fax: +1 304 285 6389.
E-mail address: DPorter@cdc.gov (D.W. Porter).

0300-483X/$ – see front matter. Published by Elsevier Ireland Ltd.
doi:10.1016/j.tox.2009.10.017

non-dose-dependent formation of multifocal granulomas. The toxicological significance of these granulomas was questioned because their formation was possibly due to the instillation of a bolus of agglomerated SWCNT. A later study reported that exposure of mice, by pharyngeal aspiration to SWCNT, caused transient, dose-dependent inflammation (Shvedova et al., 2005). After exposure, both compact aggregates and dispersed structures were observed in the lung. Dense aggregates of SWCNT were associated with foci of granulomatous inflammation, including discrete granulomas with hypertrophic epithelial cells. Interstitial fibrosis was prevalent in areas that did not have these aggregates, indicating dispersed SWCNT as the cause. The fibrosis developed rapidly and was progressive post-exposure. Using a filter to select dispersed SWCNT, it was possible to demonstrate that dispersed SWCNT are rapidly incorporated into the alveolar interstitium and produce a generalized fibrotic response (Mercer et al., 2008). A subsequent inhalation study in mice demonstrated that inflammation was a feature of mice exposed by either inhalation or pharyngeal aspiration (Shvedova et al., 2008).

In vivo studies of MWCNT are very limited, and the results of these studies are not consistent. Pulmonary clearance of MWCNT in mouse lung, after intratracheal exposure, has been examined using ^{14}C-taurine-labeled MWCNT (Deng et al., 2007). This study reported that lung burden deceased from 78% to 20% total exposed dose from 1 day to 28 days post-exposure, indicating the mouse lung can clear MWCNT. However, the retained 20% lung burden in this study also demonstrates that a subfraction of MWCNT persists for at least 28 days after exposure. The pulmonary toxicity of MWCNT in rats exposed by IT instillation to whole (5.9 μm long) or ground (0.7 μm long) reported both MWCNT samples caused acute pulmonary inflammation at 3 and 15 days post-exposure, and induced pulmonary fibrosis at 60 days post-exposure (Muller et al., 2005). In contrast, inhalation exposure of mice to MWCNT has been reported to induce no significant lung toxicity, but did cause immunosuppression (Mitchell et al., 2007). The different findings in these two studies have been attributed to differences in MWCNT surface area, rodent species used, and differences in observation period (McDonald and Mitchell, 2008). Alternatively, it has been suggested that the nanoparticles used in the inhalation study (Mitchell et al., 2007) were carbon nanofibers, not MWCNT (Lison and Muller, 2008).

Because of the paucity of data regarding possible adverse health outcomes resulting from exposure to MWCNT, we investigated the pulmonary toxicity of an occupationally relevant MWCNT exposure. Specifically, we conducted an in vivo dose-response and time course study of MWCNT in mice in order to assess their ability to induce pulmonary inflammation, damage, and fibrosis.

2. Methods

2.1. MWCNT

MWCNT used in this study were obtained from Mitsui & Company (MWNT-7, lot #05072001K28).

2.2. High resolution transmission electron microscopy

The morphology and the lattice images of MWCNT were recorded using Philips CM 20 transmission electron microscope (TEM) equipped with EDS (EDAX/4pi). TEM specimens were prepared by a standard method for powder samples. The MWCNT were dispersed into ethanol with assistance of sonication. And then a droplet of MWCNT suspension was pipetted onto a carbon coated copper grid, and followed up with drying in ambient air at room temperature prior to TEM observation.

2.3. Low resolution transmission electron microscopy

Suspensions of MWCNT were prepared in dispersion medium (DM; Ca^{2+} and Mg^{2+}-free phosphate buffered saline, pH 7.4, supplemented with 5.5 mM D-glucose, 0.6 mg/ml mouse serum albumin, and 0.01 mg/ml 1,2-dipalmitoyl-sn-glycero-3-phosphocholine) as previously described by our laboratory (Porter et al., 2008). After suspension in DM an aliquot of MWCNT sample was diluted 1:1000 with dH_2O for imaging by transmission electron microscopy. A drop (approximately 0.1 ml) was deposited onto a formvar-coated copper grid and allowed to air dry. Images were photographed on a JEOL 1220 transmission electron microscope.

2.4. Scanning electron microscopy

For scanning electron microscopy, the fixed lungs were paraffin embedded, sectioned at 8 μm, placed on carbon planchets, deparaffinized and sputter coated. After coating the specimens were examined with a Hitachi Model S-4800 field emission scanning electron microscope (FESEM) between 5 and 20 kV.

2.5. MWCNT trace metal analyses

To determine trace metals, bulk samples of MWCNT were digested by nitric/perchloric acid ashing procedure (NIOSH). The residues were dissolved in 10.0 ml of 4% HNO_3–1% $HClO_4$ for trace metals analysis by inductively coupled plasma-optical emission spectroscopy.

2.6. MWCNT endotoxin analyses

To determine endotoxin, bulk samples of MWCNT were prepared as 1.8 mg/ml suspensions in water. After rocking on a platform at room temperature for 24 h, the samples were centrifuged (5000 × *g*, 10 min, room temperature) for 10 min. Next, the samples were filtered using 0.45 μm syringe filter to remove any remaining particulate. Endotoxin analyses were done using the Limulus amebocyte lysate assay (Kinetic-QCL, BioWhittaker, Walkersville, MD).

2.7. XPS analyses of MWCNT

X-ray photoelectron spectroscopy (XPS) analyses were performed with a PHI 5000 Versa Probe (Physical Electronics, MN). Prior to XPS measurement, the MWCNT were pressed to form a pellet, and then the pellet was put into the entry-load chamber to pump for 6 h. Photoemission was stimulated by a monochromated Al Kα radiation (1486.6 eV). Survey scan and high-resolution scan were collected using pass energies of 94 and 58 eV, respectively. Binding energies of spectra were referenced to the C 1s binding energy set at 284.6 eV for the carbon nanotubes.

2.8. Determination of MWCNT zeta potential

Suspensions of MWCNT were prepared in DM as previously described by our laboratory (Porter et al., 2008). The surface charge of the MWCNT was measured with a Malvern Zetasizer Nano ZS instrument. For these experiments the electrophoretic mobility was converted into the zeta potential by means of the Schmolukowski relation.

2.9. ESR analyses

All electron spin resonance (ESR) measurements were conducted using a Bruker Instruments (Billerica, MA) EMX ESR spectrometer and a flat cell assembly. Hyperfine couplings were measured (to 0.1 G) directly from magnetic field separation using potassium tetraperoxochromate (K_3CrO_8) and 1,1-diphenyl-2-picrylhydrazyl (DPPH) as reference standards. The Acquisit program (Bruker Instruments, Billerica, MA) was used for data acquisition and analysis. Each assay consisted of 100 mM 5,5-dimethyl-1-pyrroline-*N*-oxide (DMPO), 0.1 or 1 mM $FeSO_4$, 0.1 or 1 mM hydrogen peroxide (H_2O_2), and ±MWCNT (0.8 mg/ml) in a total volume of 1 ml DM.

2.10. Animals

Male C57BL/6J mice (7 weeks old) were obtained from Jackson Laboratories (Bar Harbor, ME). Mice were housed one per cage in polycarbonate isolator ventilated cages, which were provided HEPA-filtered air, with fluorescent lighting from 0700 to 1900 h. Autoclaved Alpha-Dri virgin cellulose chips and hardwood Beta-chips were used as bedding. Mice were monitored to be free of endogenous viral pathogens, parasites, mycoplasms, Helicobacter and CAR Bacillus. Mice were maintained on Harlan Teklad Rodent Diet 7913 (Indianapolis, IN), and tap water was provided ad libitum. Animals were allowed to acclimate for at least 5 days before use. All animals used in this study were housed in an AAALAC-accredited, specific pathogen-free, environmentally controlled facility.

2.11. MWCNT pharyngeal aspiration exposure

Suspensions of MWCNT were prepared in DM as previously described by our laboratory (Porter et al., 2008). Mice were anesthetized with isoflurane (Abbott Laboratories, North Chicago, IL). When fully anesthetized, the mouse was positioned with its back against a slant board and suspended by the incisor teeth using a rubber band. The mouth was opened, and the tongue gently pulled aside from the oral cavity. A 50 μl aliquot of sample was pipetted at the base of the tongue, and the tongue was restrained until at least two deep breaths were completed (but for not longer than 15 s). Following release of the tongue, the mouse was gently lifted off

the board, placed on its left side, and monitored for recovery from anesthesia. Mice received either DM (vehicle control), 10, 20, 40 or 80 μg MWCNT.

2.12. Bronchoalveolar lavage

At 1, 7, 28 and 56 days post-exposure, mice were euthanized with an i.p. injection of sodium pentobarbital (>100 mg/kg body weight) followed by exsanguination. A tracheal cannula was inserted and bronchoalveolar lavage (BAL) was performed through the cannula using ice cold Ca^{2+} and Mg^{2+}-free phosphate buffered saline, pH 7.4, supplemented with 5.5 mM D-glucose (PBS). The first lavage (0.6 ml) was kept separate from the rest of the lavage fluid. Subsequent lavages, each with 1 ml of PBS, were performed until a total of 4 ml of lavage fluid was collected. BAL cells were isolated by centrifugation (650 × *g*, 5 min, 4 °C). An aliquot of the acellular supernatant from the first BAL (BAL fluid) was decanted and transferred to tubes for analysis of lactate dehydrogenase (LDH) and albumin. The acellular supernatants from the remaining lavage samples were decanted and discarded. BAL cells isolated from the first and subsequent lavages for the same mouse were pooled after resuspension in PBS, centrifuged a second time (650 × *g*, 5 min, 4 °C), and the supernatant decanted and discarded. The BAL cell pellet was then resuspended in PBS and placed on ice. Total BAL cell counts were obtained using a Coulter Multisizer 3 (Coulter Electronics, Hialeah, FL) and cytospin preparations of the BAL cells were made using a cytocentrifuge (Shandon Elliot Cytocentrifuge, London). The cytospin preparations were stained with modified Wright-Giemsa stain and cell differentials were determined by light microscopy.

2.13. BAL fluid LDH and albumin measurements

BAL fluid LDH activities were evaluated as a marker of cytotoxicity. BAL fluid LDH activities were determined by monitoring the LDH catalyzed oxidation of lactate to pyruvate coupled with the reduction of NAD at 340 nm using a commercial assay kit (Roche Diagnostics Systems, Montclair, NJ). Both the BAL fluid albumin and LDH assays were conducted using a COBAS MIRA Plus (Roche Diagnostic Systems, Montclair, NJ).

2.14. Histopathology

The histopathology portion of this study was designed to determine the location of aspirated MWCNTs within the lung, provide anatomic localization for cytotoxicity and inflammation noted by BAL, and evaluate the potential for MWCNT-induced pulmonary fibrosis. Mice for histopathology were not lavaged. To determined dose-response for histopathologic alterations, the 0, 10, 20, 40, and 80 μg exposure groups were evaluated at 7 and 28 days post-exposure. To evaluate resolution, persistence or progression of the histopathologic alterations, mice from the 0, 20 and 80 μg exposure groups were evaluated at 56 days post-exposure. Four mice were randomly assigned to each group, resulting in a total of 52 mice in this portion of the study.

Mice were euthanized by an overdose of pentobarbital (>100 mg/kg body weight, i.p.) followed by transection of the abdominal aorta to provide exsanguination. The lungs were rapidly removed and fixed by intratracheal perfusion with 1 cc of 10% neutral buffered formalin. Lungs were trimmed the same day, processed overnight in a tissue processor, and embedded in paraffin. The left lung lobe was stained with hematoxylin and eosin for routine morphologic assessment and with Sirius Red for evaluating fibrosis. To evaluate mucous metaplasia in airway epithelium, Alcian Blue/PAS pH 2.5 stains were conduct on the left lung lobes from all mice in the 56 days post-exposure groups and on 3–4 lungs for each of the comparable exposures (0, 20 and 80 μg) at the 7 days post-exposure groups. All slides were evaluated by a board-certified veterinary pathologist (AFH).

2.15. Immunofluorescence for podoplanin

Particle clearance in the lung involves transport to the lung associated lymph nodes via the pulmonary lymphatics (Harmsen et al., 1987, 1985; Morrow, 1972). The pulmonary lymphatics are localized around the vasculature, around the bronchi and bronchioles, and within or beneath the pleura (Ohtani and Ohtani, 2008). However, there is a paucity of information on the lymphatic vessels of the mouse lung (Dixon et al., 1999). In addition, reliable imaging of lymphatics in normal microscopic sections requires specific markers (Baluk and McDonald, 2008).

To visualize the lymphatics in this study, podoplanin was used as a marker for lymphatic endothelium (Baluk and McDonald, 2008) and was demonstrated using indirect immunofluorescence (see below). Normal pulmonary architecture was demonstrated using indirect immunofluorescence for e-cadherin which demonstrates intercellular adhesions in epithelium. In addition, because the e-cadherin antibodies were mouse monoclonal antibodies, the secondary donkey anti-mouse antibodies also demonstrates sites of mouse IgG deposition, including in plasma cells and in plasma in the vasculature. DAPI was used to demonstrate nuclei throughout the lung section. Using this technique, mesothelium and lymphatic endothelium stain brilliant red but can be distinguished by location, alveolar type I cells stain orange due to low levels of both podoplanin, while bronchiolar epithelium can be visualized by the green fluorescence of the epithelial adhesions, blood plasma stains green within the lumen of the vasculature, and plasma cells are brilliant green.

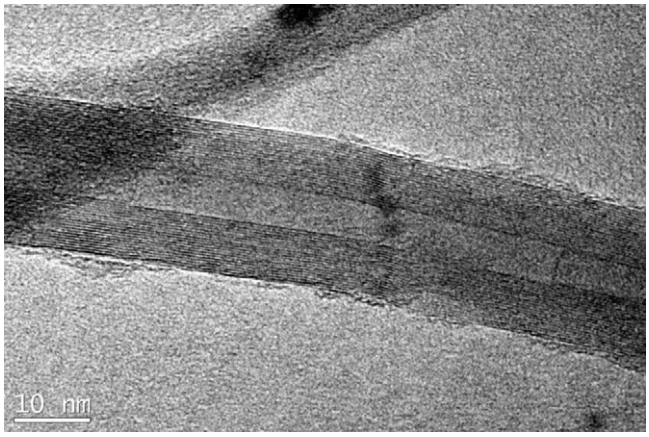

Fig. 1. High resolution transmission electron micrograph of MWCNT. A representative high resolution transmission electron micrograph of the MWCNT shows the distinctive crystalline structure of MWCNT, with this particular MWCNT having 20 walls.

For the podoplanin indirect immunofluorescence, 5 μm sections of the left lung lobe were mounted on Probe-On Plus slides (Fisher Scientific, Pittsburgh, PA). Slides were deparaffinized and then rehydrated using a 1 mM buffered solution of ethylenediaminetetraacetic acid disodium salt dehydrate (EDTA), pH 8.0, for heat-induced epitope retrieval (HIER). Tissues were blocked with 10% donkey serum (Jackson ImmunoResearch, West Grove, PA) for 2 h at room temperature. Hamster anti-podoplanin (Novus Biologicals, Littleton, CO) was diluted 1:100 and mouse anti e-cadherin (BD Biosciences, San Jose, CA) was diluted 1:50 with phosphate buffered saline (PBS) containing 0.5% donkey serum. The primary antibodies were mixed together and dropped onto the sections and incubated overnight in a humidity chamber at 4 °C. For negative controls, the primary antibodies were replaced with control mouse serum (Santa Cruz Biotechnologies, Santa Cruz, CA) and control sheep serum (Alpha Diagnostics, San Antonio, TX) at the same concentrations. The slides were rinsed with PBS then blocked again with 10% donkey serum for 30 min. Secondary antibodies, DyLight (TM) 594 goat anti-Syrian Hamster (Jackson ImmunoResearch, West Grove, PA) and Alexa-488 conjugated donkey anti-mouse (Invitrogen, Carlsbad, CA) were diluted and mixed together for a final dilution of 1:50. Secondary antibodies were dropped on to the sections and incubated in a humidity chamber at room temperature for 2 h in the dark. Slides were rinsed with PBS then coverslipped using Prolong with Dapi (Invitrogen, Carlbad, CA).

2.16. Statistics

Statistical comparisons between treatment conditions (e.g., doses) were performed separately for each post-exposure time using analysis of variance (ANOVA) with post hoc *t*-tests for pair-wise comparison of dose groups. Since variance estimates were different across dose groups, the ANOVA models were estimated using an unequal variance model available from SAS PROC MIXED (Littell et al., 1996). All statistical tests were two tailed with significance level equal to 0.05.

Since the pathology data consisted of ordinal scores then comparisons between control and MWCNT doses at each time and comparisons across time for each exposure group were accomplished using two separate one-way nonparametric analyses or variance (ANOVAs). Exact test were used because of the high number of tied values in the data. The nonparametric ANOVA was performed using SAS Proc NPAR1WAY with exact Kruskal–Wallace tests for multi-group comparisons and exact Wilcoxon tests for post hoc pair-wise comparisons. All statistical tests were two tailed and performed at the 0.05 significance level.

3. Results

3.1. Characterization of bulk MWCNT

Several different analyses were performed to characterize the MWCNT. High resolution transmission electron microscopy (TEM) images showed the distinctive crystalline structure of MWCNT, with the number of walls ranging from 20 to 50 walls (Fig. 1). Overall MWCNT trace metal contamination was 0.78%, with sodium (0.41%) and iron (0.32%) being the two major metal contaminants with no other metals present above 0.02%. Endotoxin contamina-

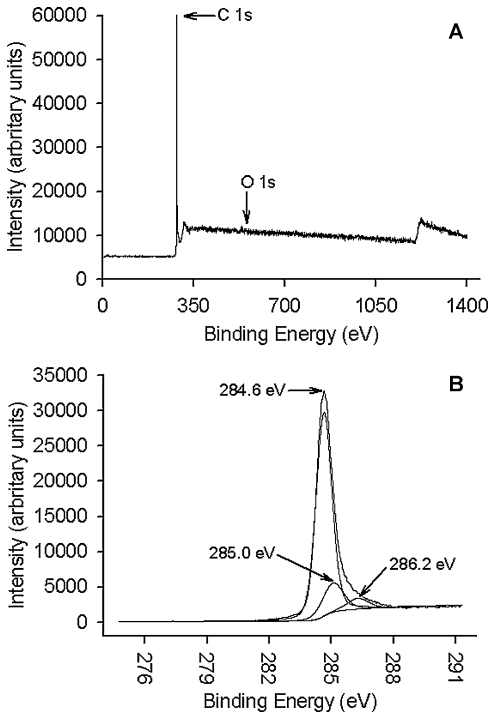

Fig. 2. XPS spectra of MWCNT. XPS survey-scan spectrum (panel A) has a dominant carbon (C 1s) peak and a small oxygen (O 1s) peak. The detailed-scan XPS spectrum (panel B) of the C 1s core level determined a C 1s peak at 284.6 and 285 eV which corresponds to the sp2-hybridised graphite-like carbon atoms of the carbon nanotube and the sp3-hybridised carbon atoms with disordered structure, respectively. The C 1s peak component at 286.2 eV is attributed to the C–O bond, indicating the formation of the hydroxyl groups on the MWCNT surface.

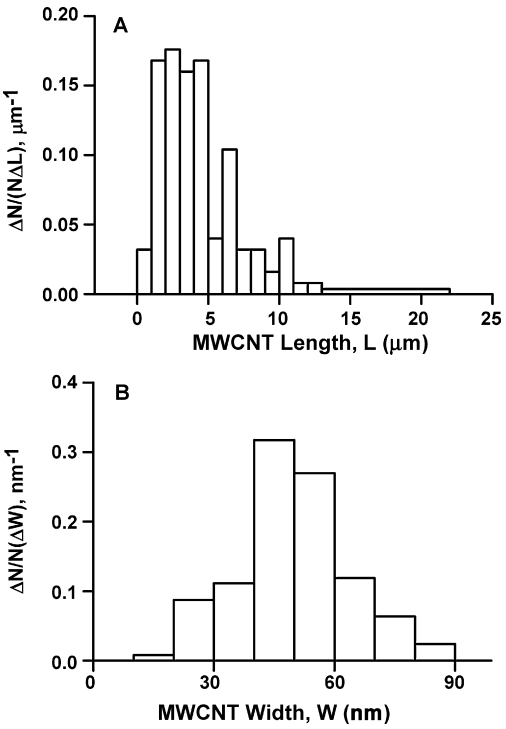

Fig. 4. Length and width size distribution of hydrosol MWCNT. MWCNT length distribution was log normal, with median length of 3.86 μm (GSD 1.94) (panel A). MWCNT width distribution followed normal distribution, with count mean width of 49 ± 13.4 (S.D.) (panel B).

tion of the MWCNT was tested and determined to be below the level of detection.

X-ray photoelectron spectroscopy measurement was performed on the MWCNT samples. The survey-scan spectrum obtained from the MWCNT sample (Fig. 2A) has a dominant C 1s peak, and a small amount of oxygen was also detected. No other elements were found by XPS measurements. The detailed-scan XPS spectrum (Fig. 2B) of the C 1s core level determined a C 1s peak at 284.6 eV.

3.2. Characterization of hydrosol MWCNT

Representative TEM micrographs of MWCNT dispersed in PBS (Fig. 3A) and DM (Fig. 3B) from this study support the conclusion that DM promotes dispersion of MWCNT (Porter et al., 2008). MWCNT width distribution followed normal distribution, whereas the MWCNT length distribution was log normal. MWCNT physical parameters, i.e., width and length, were determined from TEM micrographs of dispersed MWCNT and determined MWCNT median length of 3.86 μm (GSD 1.94) (Fig. 4, panel A) and count mean width of 49 ± 13.4 (S.D.) nm (Fig. 4, panel B).

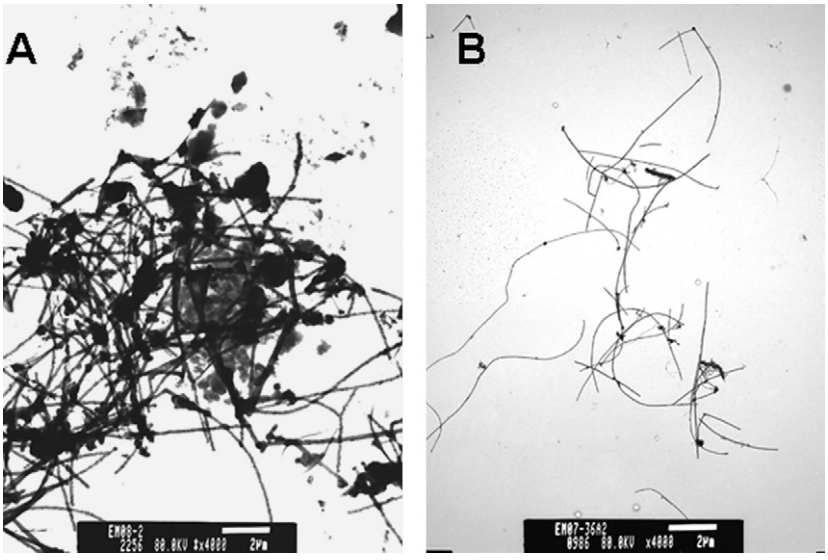

Fig. 3. Dispersion of MWCNT in PBS and DM. Representative TEM micrograph of MWCNT dispersed in PBS (panel A) shows large agglomerates, whereas MWCNT suspended in DM (panel B) are much better dispersed.

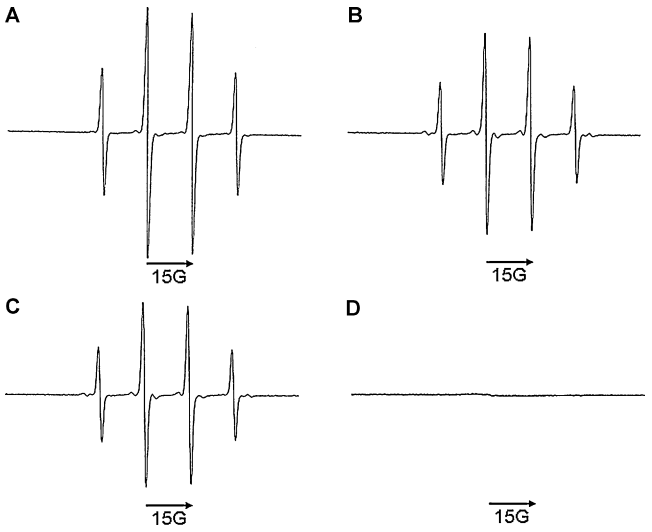

Fig. 5. ESR study of MWCNT. Panel A, PBS with 100 mM DMPO + 0.1 mM $FeSO_4$ + 1 mM H_2O_2. Panel B, DM with 100 mM DMPO + 0.1 mM $FeSO_4$ + 1 mM H_2O_2. Panel C, DM with 100 mM DMPO + 0.1 mM $FeSO_4$ + 1 mM H_2O_2 + 0.8 mg/ml MWCNT. Panel D, DM with 100 mM DMPO + 1 mM H_2O_2 + 0.8 mg/ml MWCNT. All ESR spectra were obtained using the following settings: center field = 3480 G, sweep width = 100 G, microwave frequency = 9.794 GHz, microwave power = 20.120 mW, receiver gain = 10,000, and signal channel time constant = 40.960 ms.

The zeta potential of the MWCNT in DM was determined to be −11 mV.

3.3. Electron spin resonance studies

Acellular ESR experiments were conducted to determine if MWCNT produce reactive oxygen species (ROS). The Fenton reaction ($Fe^{2+} + H_2O_2 \rightarrow Fe^{3+} + {}^{\bullet}OH + {}^{-}OH$) was used as a source of $^{\bullet}OH$ radicals. An aqueous solution containing Fe^{2+}, H_2O_2, and a spin trap (DMPO) in a phosphate buffered saline (pH 7.4) generated a 1:2:2:1 quartet with hyperfine splittings of 15 G (Fig. 5A). Based on these splitting constants, the 1:2:2:1 quartet was assigned to a DMPO/$^{\bullet}OH$ adduct, as indirect evidence for $^{\bullet}OH$ generation. When DM was used as the aqueous buffer instead of PBS, there was a small decrease in ESR signal, indicating a small decrease in $^{\bullet}OH$ generation (Fig. 5B). Addition of MWCNT to the reaction mixture further decreased ESR signal, indicating that MWCNT were scavenging $^{\bullet}OH$ being generated from the Fenton reaction (Fig. 5C). Finally, when MWCNT were substituted for Fe^{2+} in the reaction, no $^{\bullet}OH$ generation was detected, indicating the iron present in MWCNT was not capable of generation ROS (Fig. 5D).

3.4. Bronchoalveolar lavage (BAL) studies

In order to investigate the pulmonary toxicity of MWCNT, mice were exposed by pharyngeal aspiration to DM (vehicle), or MWCNT (10, 20 or 40 μg/mouse) and BAL studies were conducted at 1, 7, 28 and 56 days post-exposure. Pulmonary inflammation was assessed by determining BAL polymorphonuclear leukocytes (PMNs). At 1 day post-exposure, BAL PMNs were significantly increased relative to vehicle-exposed controls (Fig. 6, Panel A). At 7 days post-exposure BAL PMNs exhibited a dose-response to MWCNT, and PMNs levels had increased for mice exposed to 20 and 40 μg MWCNT relative to 1-day post-exposure levels. In contrast, mice that received 10 μg MWCNT had decreased to vehicle-exposed control levels at 7 days post-exposure. At 28 days post-exposure, BAL PMNs determined for MWCNT-exposed mice

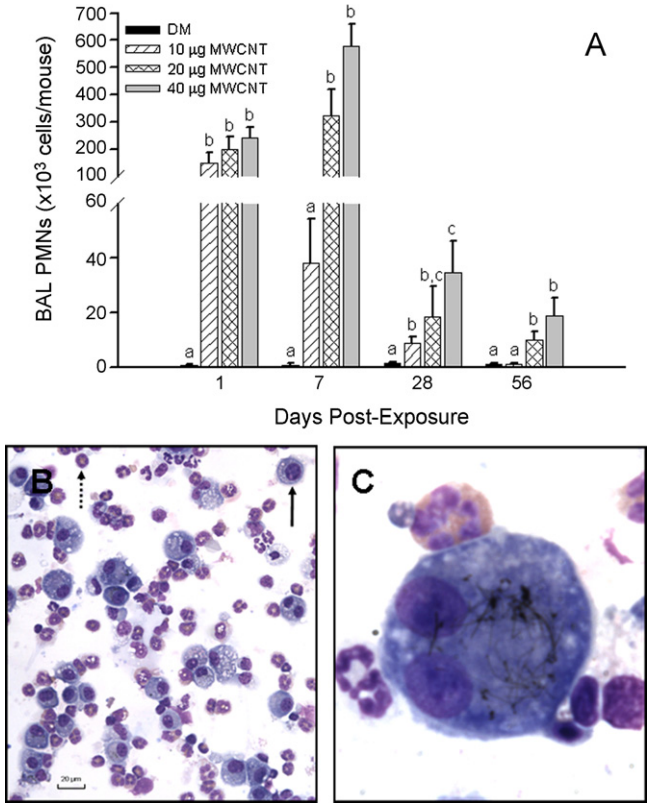

Fig. 6. Pulmonary inflammation induced by exposure to MWCNT. Mice were exposed by pharyngeal aspiration to DM (vehicle), or MWCNT (10, 20 or 40 μg/mouse) and BAL studies were conducted at 1, 7, 28 and 56 days post-exposure. Pulmonary inflammation was assessed by determining BAL polymorphonuclear leukocytes (Panel A). Light micrographs of BAL cell cytospins obtained at 7 days post-exposure from a mouse exposed to 40 μg MWCNT shows presence of numerous PMNs (dashed arrow) and AMs (solid arrow) (panel B, 40×), and an AM loaded with MWCNTs (panel C, 200×).

were lower relative to 1 and 7 days post-exposure levels, but consistently remained significantly higher than vehicle-exposed controls at 40 μg MWCNT dose. By 56 days post-exposure, mice which received 40 μg MWCNT still had increased levels of BAL PMNs. Light micrographs of BAL cell cytospins obtained at 7 days post-exposure from a mouse exposed to 40 μg MWCNT (Fig. 6, panel B) shows many PMNs. In addition, the AMs from the MWCNT-exposed mice are loaded with MWCNT (Fig. 6, panel C), indicating the MWCNT are being phagocytized by the AMs.

MWCT-induced lung damage was assessed by measuring acellular BAL fluid lactate dehydrogenase activities as a measure of cytotoxicity, and albumin concentrations as a measure of the integrity of the alveolar–blood barrier. At 1 day post-exposure, BAL fluid LDH and albumin obtained from MWCNT-exposed mice were significantly increased relative to vehicle-exposed controls (Fig. 7). At 7 days post-exposure BAL fluid LDH activities and albumin concentrations exhibited a dose-response to MWCNT, and increased for mice exposed to 20 and 40 μg MWCNT relative to 1-day post-exposure levels, whereas mice that received 10 μg MWCNT decreased relative to vehicle-exposed controls. At 28 days post-exposure, BAL fluid LDH and albumin determined for MWCNT-exposed mice were lower relative to 1 and 7 days post-exposure values, but consistently remained significantly higher than vehicle-exposed controls at 40 μg MWCNT dose. By 56 days post-exposure, mice which received 40 μg MWCNT still had increased levels of BAL fluid LDH and albumin, relative to vehicle-exposed controls.

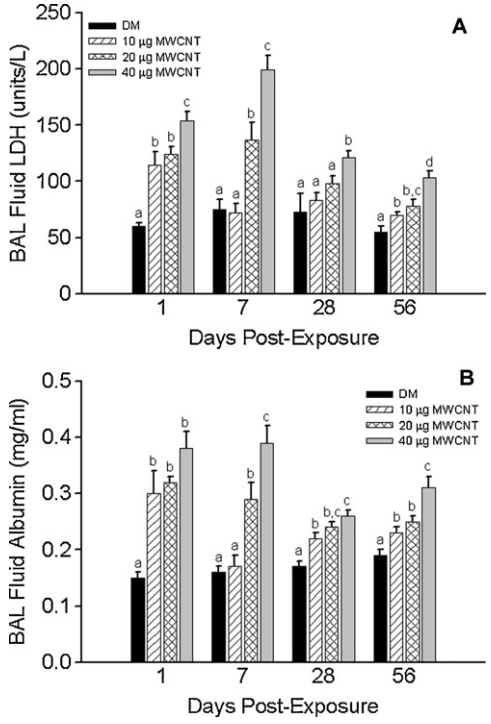

Fig. 7. BAL fluid LDH activities and albumin concentration. Mice were exposed by pharyngeal aspiration to DM (vehicle), or MWCNT (10, 20 or 40 μg/mouse) and BAL fluid was obtained at 1, 7 28 and 56 days post-exposure. BAL fluid LDH activities (panel A) and albumin concentrations (panel B) were determined.

3.5. FESEM examination of MWCNT-exposed lungs

FESEM examination of MWCNT demonstrated that the aspiration dose was widely distributed throughout the lungs and rapidly incorporated into the alveolar walls and alveolar cells (Fig. 8A and B). Engulfment of MWCNT by alveolar epithelial cells as well as alveolar macrophages was observed within one hour of aspiration (Fig. 8A). Capture of MWCNT by the alveolar epithelium occurred across the entire surface of type I alveolar epithelial cells and was not restricted to cell–cell junctions. At later time points MWCNTs were generally no longer present on the surface of epithelial cells but had been transported within the alveolar interstitium and/or interstitial cells and within alveolar macrophages (Fig. 8B). As illustrated in Fig. 8B, alveolar macrophages were loaded with MWCNT and many of the CNT protruded from the macrophage for days and weeks after aspiration.

3.6. Histopathology

The principal morphologic changes in MWCNT-exposed lungs were granulomatous to pyogranulomatous, proliferative bronchointerstitial pneumonia and pleuropneumonia. By histopathology, the inflammation was pleocellular at early time points and the major inflammatory cell was the macrophage with lesser numbers of giant cells, neutrophils, and eosinophils. By day 56, peribronchiolar aggregates of lymphocytes and plasma cells were sometimes seen in the highest exposure groups. Macrophages frequently had more than one nucleus and some macrophages had no nuclei. Prominent giant cells were seen in some exposed mice at all time points but had cellular atypia characterized by variations in nucleolar prominence, chromatin condensation and nuclear size (Fig. 9A). Inflammation often involved the interstitium and sometimes extended from the interstitium into the lumen at the bronchioloalveolar junction, resulting in a potentially obstructive change. In addition, the bronchioles themselves

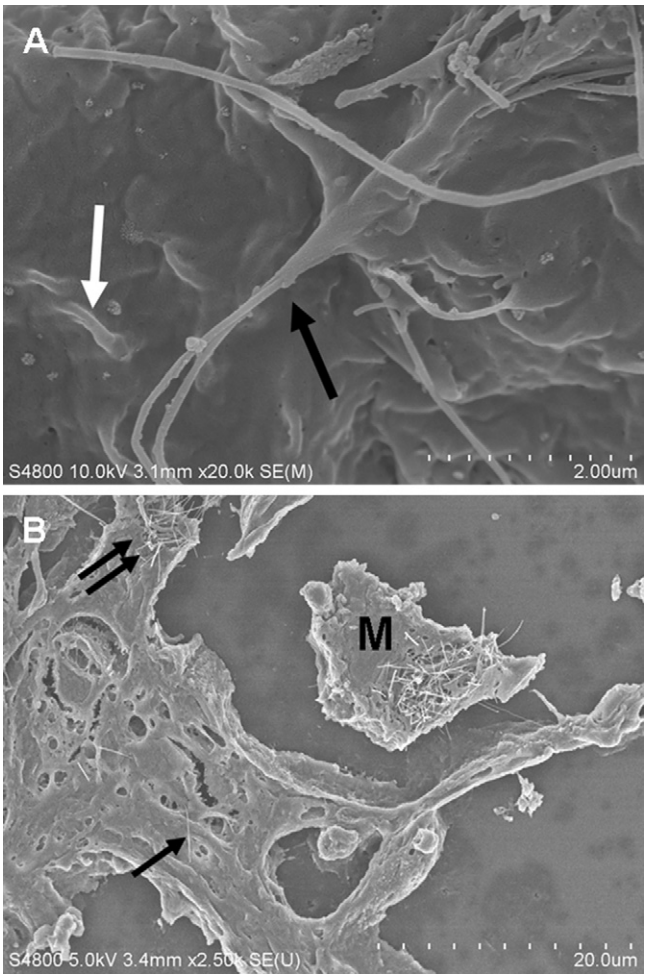

Fig. 8. FESEM of MWCNT in lungs. (A) The initial stages of MWCNT capture by the alveolar epithelial surface 1 day after aspiration of a 10 μg dose. Partial engulfment of several MWCNTs is visible (black arrows) while others appear to be outlined below the surface (white arrows). Free-ends of the MWCNT are also visible. The section image in B demonstrates the distribution of MWCNT within the alveolar walls and alveolar macrophages 28 days after aspiration. MWCNT in the interstitium ranged from single fibers (arrow) to larger clusters (double arrows). Alveolar macrophage (M). FESEM of 5 μm paraffin section of mouse lung.

were involved in the inflammatory and proliferative pulmonary response. The generally bronchiolocentric inflammation persisted throughout the 56-day post-exposure period (Fig. 9B). Bronchiolar and alveolar epithelial cells of MWCNT-exposed lungs had morphologic changes consistent with hyperplasia and hypertrophy (Fig. 10A and B). Cellular atypia was also a frequent characteristic of the hypertrophied and hyperplastic bronchiolar epithelial cells and some hypertrophied alveolar epithelial cells (Fig. 10B and C). Alcian Blue-Periodic Acid Schiff staining of representative sections in the 20 and 80 μg exposure groups demonstrated mucous metaplasia at day 7 with persistence through day 56 post-exposure (Fig. 10C). The overall histopathology of the MWCNT-exposed lung was consistent with granulomatous to pyogranulomatous, proliferative bronchointerstitial pneumonia and pleuronemonia but was somewhat reminiscent of proliferative bronchiolitis obliterans-organizing pneumonia (BOOP) as described in humans (Epler, 1992, 2001; Epler et al., 1985; Ryu et al., 2003). Fibrosis accompanied the organizing pulmonary inflammation and was seen at 7 days post-exposure and persisted through day 56 post-exposure (Fig. 11A and B). Fibrosis was most easily demonstrated within discrete granulomas but was also seen in inflamed alveolar septa without discrete granulomas.

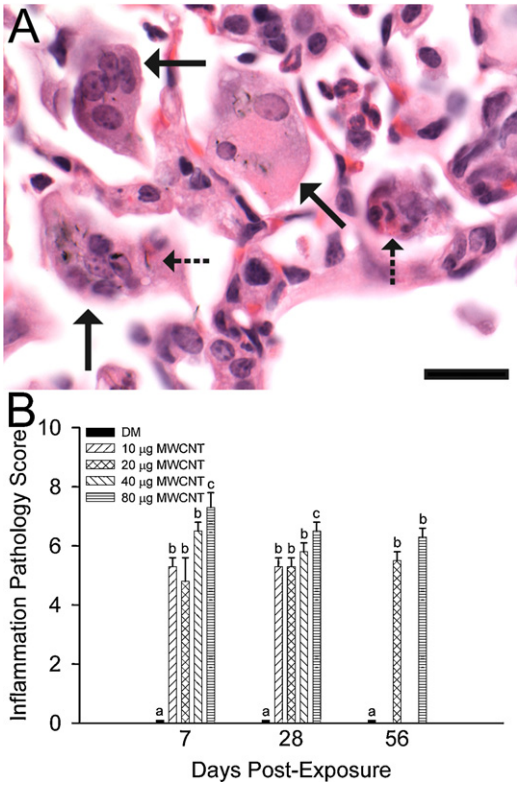

Fig. 9. Inflammation in the MWCNT-exposed lung. (A) A photomicrograph from the lung of a mouse 7 days after aspirating 40 μg MWCNT. The inflammation is pleocellular and includes macrophages, eosinophils, neutrophils and atypical giant cells with anisokaryosis (solid arrows). The giant cells also sometimes contained inflammatory cell debris (dashed arrows) and MWCNT. Inflammation involves both the interstitium and the alveolar space. H&E stain. Bar is 20 μm. (B) Bar graph showing the persistence of inflammation after exposure.

Inflammation extended from the centra-acinar lung to the pleura in just over half of the MWCNT-exposed mice. The pleura was involved in MWCNT-induced inflammation in one mouse exposed to 10 μg, all mice exposed to 20 or 40 μg, and three of four mice exposed to 80 μg. At 28 days post-exposure, inflammation extended to the pleura in two mice exposed to 10 μg, two of four mice in the 20 and 40 μg groups, and three of four mice exposed to 80 μg (Fig. 12A and B). At 56 days post-exposure, inflammation extended to the pleura in two of four mice exposed to 20 and 80 μg. At 56 days post-exposure in two mice in the 80 μg exposure group, MWCNTs penetrated the pleura (Fig. 13A). In some sections, peribronchiolar and/or subpleural lymphatics were dilated (Fig. 13B and C). In addition, by 56 days post-exposure, the peribronchiolar lymphatics were dilated in all mice in the 80 μg and in one mouse in the 20 μg exposure group but in none of the controls (Fig. 14A–C). Within the macrophages themselves and in some epithelial cells, the MWCNTs frequently penetrated the cytoplasmic membrane (Fig. 13A). In podoplanin stained sections from control mice, lymphatics in the peribronchiolar interstitium (Fig. 15A and B) and interlobular septa (Fig. 15C and D) were readily visualized as narrow, thin-walled structures without intralumenal macrophages. Subpleural lymphatics in control mice were collapsed and could not be distinguished from the pleura itself (Fig. 15D and E).

4. Discussion

The primary objective of this investigation was to evaluate MWCNT-induced pulmonary inflammation, damage, and fibrosis. To accomplish this, mice were exposed by pharyngeal aspiration to MWCNT in doses of 10, 20, 40 and 80 μg per mouse. In order to evaluate the relevance of the findings of this in vivo mouse study to human MWCNT exposures, we need to determine if the doses tested in mice are relevant human occupational exposures. Assuming a mouse alveolar epithelium surface area of 0.05 m^2 (Stone et al., 1992), the 10 μg MWCNT dose would result in 200 μg MWCNT/m^2 alveolar epithelium, whereas the 80 μg MWCNT would result in 1600 μg MWCNT/m^2 alveolar epithelium. A recent study reported peak MWCNT-containing airborne dust levels of approximately 400 μg/m^3 in a research laboratory (Han et al., 2008). Assuming a peak MWCNT aerosol of 400 μg/m^3, MWCNT mass median aerodynamic diameter (MMAD) = 1.5 μm (Porter et al., 2009), minute ventilation of 20 l/min (Galer et al., 1992) and deposition fraction of 30% (Phalen, 1984), and human alveolar epithelium surface area of 102 m^2 (Stone et al., 1992), approximate human exposure per month would be 226 μg MWCNT/m^2 alveolar epithelium. Thus, 10 μg MWCNT exposure in mouse approximates human deposition for a person performing light work for one month in a work environment with MWCNT aerosol of 400 μg/m^3. Even if the average daily MWCNT aerosol is determined to be much lower once more workplace exposure data is collected, e.g., 4–40 μg/m^3, the 10 μg MWCNT exposure in mouse would approximate human deposition for a person performing light work for approximately 9 months to 7.5 years. Thus, these estimates suggest that the MWCNT doses tested in mice in this study approximate reasonable human occupational exposures to MWCNT.

Great effort was invested in the characterization of the MWCNT used in this study because nanotoxicology studies that lack adequate nanoparticle characterization may not provide meaningful data or conclusions (Warheit, 2008). A panel of experts has recommended the characterization of both “as produced” and “as administered” nanoparticles used in toxicological studies (Oberdorster et al., 2005). Several different techniques were applied to characterize the physico-chemical properties of both the “as produced” and “as administered” MWCNT.

Importantly, because we were concerned with the effects of MWCNT inhaled by production workers, the MWCNT investigated and characterized in this study were without post-production processing, such as acid washing. The as produced, or bulk MWCNT, underwent several different analyses; (1) high resolution TEM, (2) XPS, (3) metal determinations, and (4) endotoxin content. High resolution TEM determined conclusively that the nanoparticles used in this study were MWCNT, and not some other form of carbon nanoparticle or amorphous carbon. Thus, any toxicological outcomes determined in this study can be attributed to exposure to MWCNT.

XPS analyses determined a C 1s peak at 284.6 eV that corresponds to the sp2-hybridised graphite-like carbon atoms of the nanotubes (Ago et al., 1999; Chen, 1999). The C 1s peak component at 285 eV is ascribed to the sp3-hybridised carbon atoms with the disordered structure (Pinault et al., 2005). The C 1s peak component at 286.2 eV is attributed to the C–O bond (Felten et al., 2006; Stankovich, 2006), which indicates the formation of the hydroxyl group on the nanotube surface (Felten et al., 2006). The zeta potential of the MWCNT in DM was determined to be −11 mV, which is consistent with the determination of hydroxyl groups on the MWCNT surface by XPS.

Metals, which are used as catalysts for MWCNT synthesis, can remain as contaminates in bulk CNT. The MWCNT in this study were analyzed for 31 different metals, and this analyses determined the total metal content was relatively low, 0.78%, with sodium (0.41%) and iron (0.32%) being the two major contaminates. Another contaminate of concern, endotoxin, is produced by gram negative bacteria and has the potential to contaminate many products due to the ubiquitous distribution of gram negative bacteria in the environment. Analyses of the bulk MWCNT determined that endotoxin levels were below the level of detection.

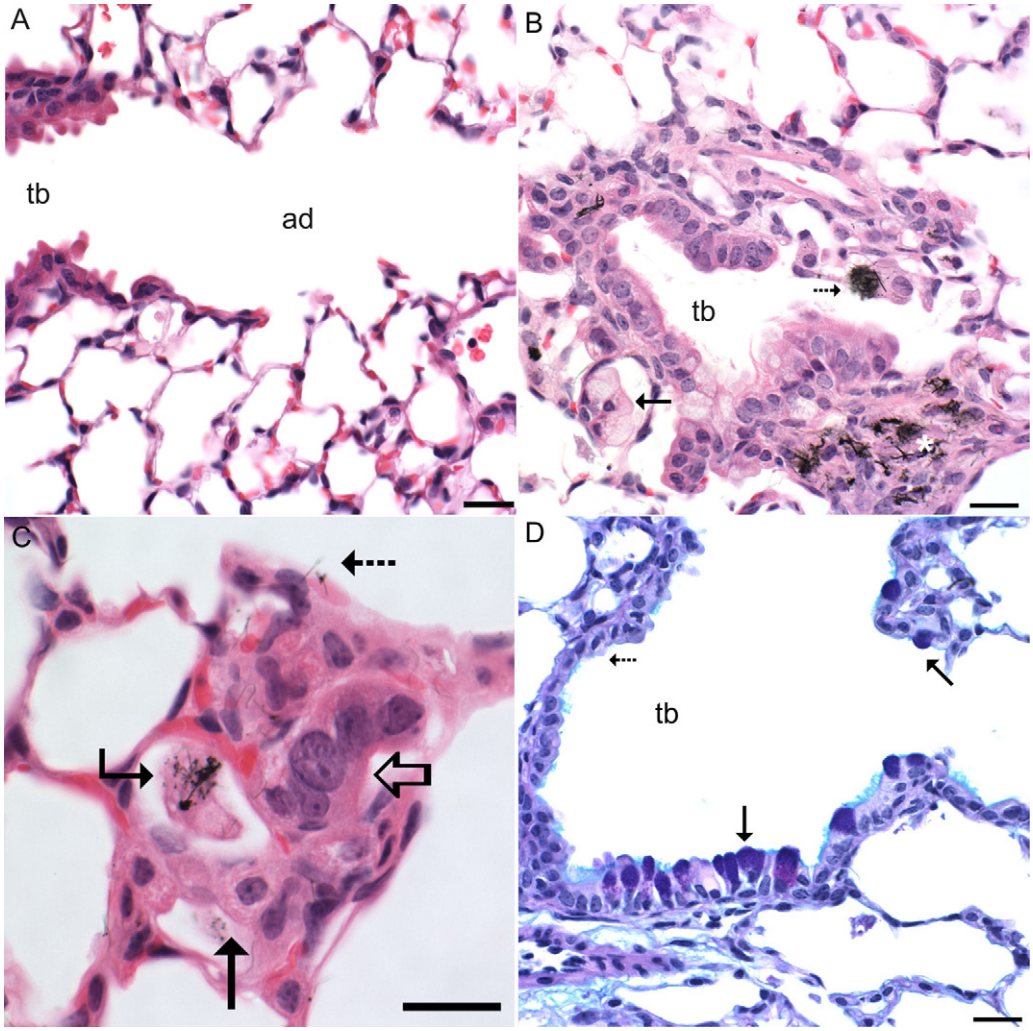

Fig. 10. Histopathology of the bronchioloalveolar region of the mouse lung. (A) The terminal bronchiole (tb) and first generation alveolar duct (ad) of a control mouse lung showing the normal low cuboidal epithelium of the terminal bronchiole, low numbers of macrophages, an absence of neutrophils and thin alveolar septa. H&E stain. (B) Photomicrograph from the lung of a mouse 56 days after aspirating 20 μg MWCNT. The epithelium lining the terminal bronchiole is hypertrophied with atypical changes which include enlarged nuclei (karyomegaly). Granulomatous inflammation (*) is in the interstitium. A focus of atypical epithelial cells (solid arrow) is in an adjacent alveolus and a bundle of MWNCT extend beyond the cytoplasmic margins of a phagocytizing macrophage. H&E stain (dashed arrow). (C) Photomicrograph from the lung of a mouse 28 days after aspirating 20 μg MWCNT. Hypertrophied alveolar type II cells line some alveoli (solid straight arrow) and adjacent to the hypertrophied type II cells is a focus of highly atypical cells (open arrow). Some MWCNT project beyond cytoplasmic margins (dashed arrow) and a macrophage with multiple intracytoplasmic MWCNT has no nucleus (bent arrow). (D) Photomicrograph from a mouse 56 days after aspirating 20 μg MWCNT. Foci of mucous metaplasia (solid arrows) are indicated by the dark purple staining with Alcian Blue/PAS while other foci of bronchiolar epithelium retain a normal morphology and, like controls, do not contain mucosubstances (dashed arrow). Bar is 20 μm.

The MWCNT in this study were prepared in aqueous suspension prior to aspiration exposure. Like its bulk counterpart, the aqueous suspension of MWCNT also underwent several different analyses to characterize its physico-chemical properties. These analyses determined dispersion status, MWCNT physical dimensions (length and width), zeta potential, and MWCNT-mediated ROS generation.

Our laboratory has previously reported that MWCNT in PBS are highly agglomerated into large masses, whereas MWCNT in DM are significantly more dispersed, based on examination of low resolution TEM micrographs (Porter et al., 2008). In this study, TEM micrographs of MWCNT prepared as aqueous suspension in DM were similar to those our lab has previously reported, confirming that the MWCNT were well dispersed, but also did contain some nanoropes composed of MWCNT. Using TEM micrographs we were also able to determine the length of MWCNT is 3.86 μm and count mean width of 49 nm. It should be noted that MWCNT which had formed nanoropes were not used for the sizing determinations, because it was impossible to determine how many MWCNT composed these nanoropes, nor the point where one MWCNT started and one ended in a particular nanorope.

In our study, MWCNT were dispersed prior to aspiration exposure using DM, a BAL fluid mimic previously described by our laboratory (Porter et al., 2008). FESEM examination of MWCNT-exposed mice demonstrated that MWCNT were widely distributed, suggesting the dispersion of the MWCNT in DM prior to exposure was successful in preventing MWCNT agglomeration in the lung. Dispersion of MWCNT was critical to this study, because a previous rat IT study of SWCNT noted that agglomeration of SWCNT resulted in mortality rate of approximately 15% within 24 h post-exposure due to SWCNT agglomerates blocking upper airways (Warheit et al., 2004). In addition, data from this same study reported that SWCNT exposure produced transient inflammation and a non-dose-dependent formation of multifocal granulomas. The toxicological significance of these granulomas

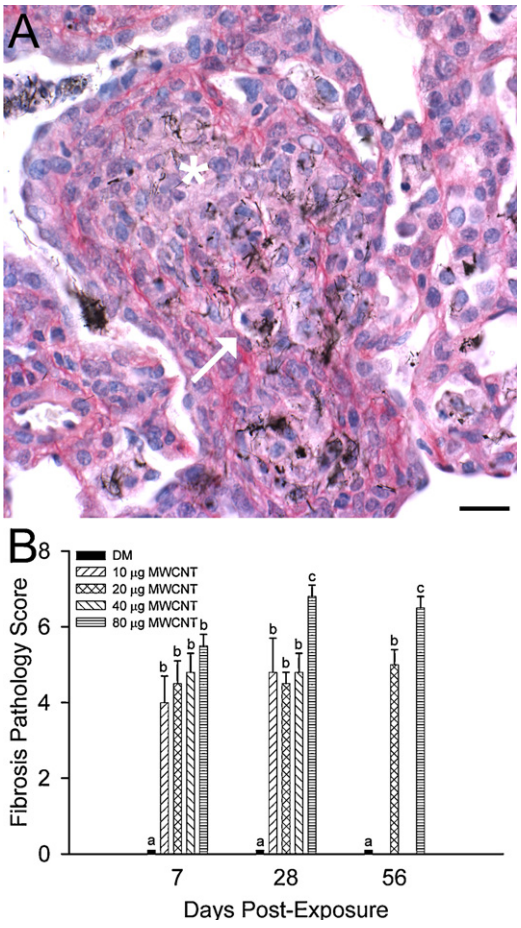

Fig. 11. MWCNT increased fibrosis in the lung of the MWCNT-exposed mouse. (A) Photomicrograph from the lung of a mouse 7 days after aspirating 80 μg MWCNT demonstrating early fibrosis by the red-staining fibers within an inflammatory granuloma (*). Numerous MWCNT are within the section and cellular replication continues in a cell despite the presence of MWCNT (arrow). (B) Semi-quantitative histopathology from Sirius Red stained sections indicate persistence of fibrosis for at least 56 days post-exposure.

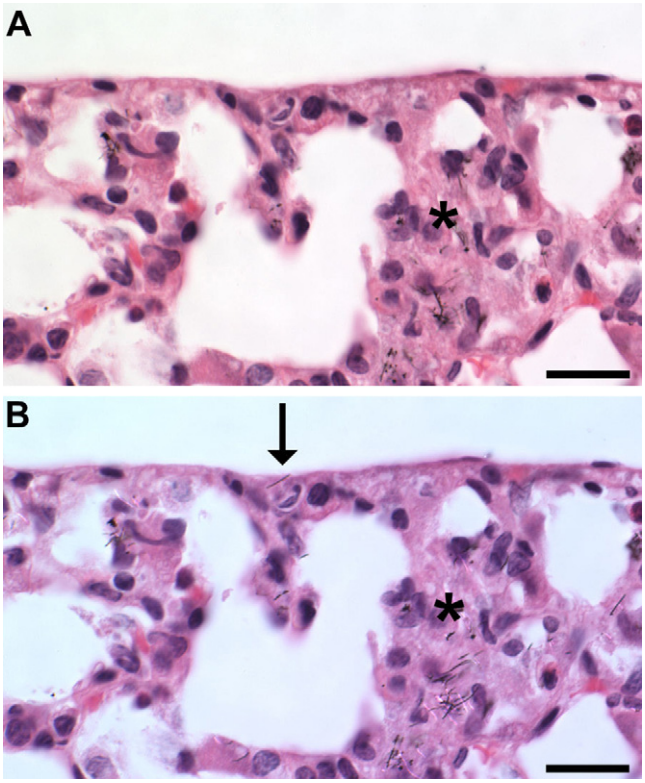

Fig. 12. Pleural inflammation in MWCNT-exposed mice. (A) Interstitial inflammation (*) extends from the interstitium to the overlying pleura in a mouse exposed to 40 μg MWCNT 7 days before sacrifice. (B) The microscopic field in panel A has been partially polarized to demonstrate additional MWCNT that are sometimes difficult to see in routine light microscopy, including a MWCNT incorporated into the pleural inflammatory response (arrow).

was questioned because their formation was possibly due to the instillation of a bolus of agglomerated nanotubes (Warheit et al., 2004).

Analyses of FESEM micrographs also demonstrated MWCNT were rapidly incorporated into the alveolar cells and walls (within one hour post-exposure), and were present in the alveolar interstitium and/or interstitial cells at later post-exposure times. AMs were also observed to be loaded with MWCNT, which is consistent with light microscopy observations made from BAL cell cytospin preparations made from MWCNT-exposed mice.

In vitro studies with NR8383 and A549 cells demonstrated dose- and time-dependent increases in intracellular ROS production after exposure to SWCNT or MWCNT, suggesting that CNT exposure induces cellular oxidative stress (Pulskamp et al., 2007). However, when the carbon nanotubes used in these experiments were acid-treated to remove metal contaminates, the cellular ROS generation did not occur, suggesting the metal catalyst contaminates were responsible for the ROS generation. The MWCNT used in these studies had low metal contamination, but did include iron, thus we had to at least consider the possibility that this iron contamination may contribute to ROS generation and MWCNT toxicity. To test ROS generation from MWCNT, cell-free ESR experiments were conducted and determined that MWCNT do not generate ROS, and in fact, scavenge ROS to a small degree. Thus, the iron present in the MWCNT is either not bioavailable, or is a form that is not redox reactive. These findings are consistent with a previous study which also determined that MWCNT in aqueous suspension do not directly generate ROS (Fenoglio et al., 2006).

The fiber-like dimensions of MWCNT have caused some researchers to hypothesize that these new nanotubes, if persistent in the lung, could cause diseases which are reminiscent of the classic inhalable occupational fiber, asbestos (Donaldson et al., 2006; Donaldson and Tran, 2004). Like asbestos fibers, our study demonstrates that MWCNT cause persistent inflammation in the lung. In BAL, this was reflected in increased PMNs, which was transient at low exposures but which persisted through day 56 at 40 μg. LDH and albumin also remained elevated at day 56 in mice exposed to 40 μg, indicating persistent cytotoxicity. Histopathology confirmed that PMNs were a component of the early inflammatory response to MWCNTs but demonstrated that the inflammation principally involved macrophages and had giant cells as a component, classic features of granulomatous inflammation (Ackermann, 2007). Histopathology of the MWCNT-exposed lung revealed persistent granulomatous inflammation at even the lowest exposure, 10 μg. This finding is important because granulomatous inflammation, like other forms of persistent lung inflammation, can cause lung injury and fibrosis (Williams and Williams, 1983). These findings are consistent with previous studies which demonstrated the importance of histopathology in evaluating persistent granulomatous inflammation in the lung (Henderson et al., 1985; Porter et al., 2007). It is unlikely that the persistent inflammation is due to aggregation of the MWCNT, since dispersion medium was used for the exposure and decreased aggregation (Porter et al., 2008). In addition, with SWCNT exposure, inhalation is

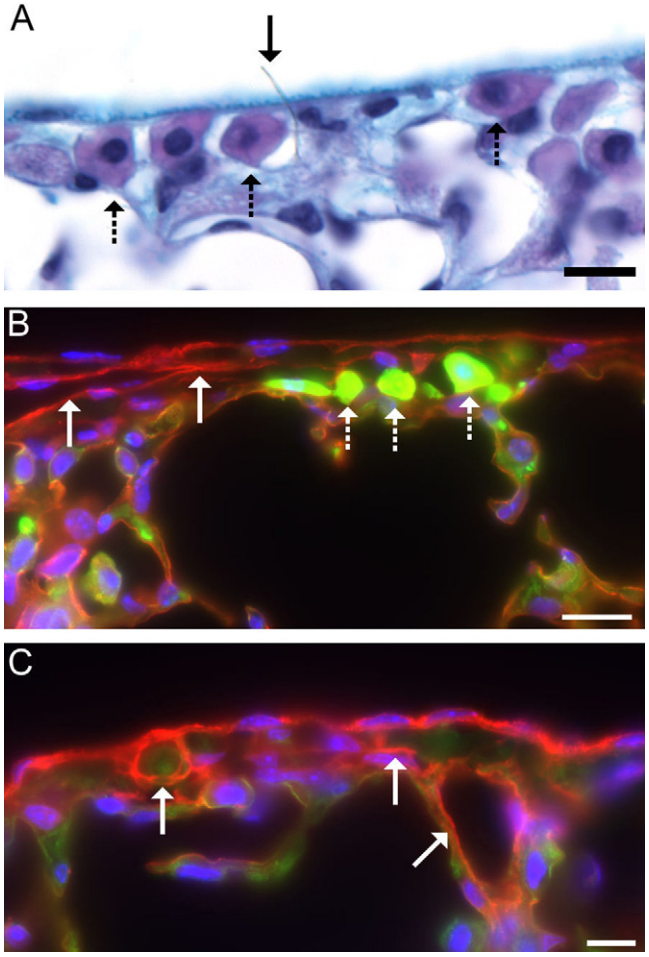

Fig. 13. Pleura migration of MWCNT. (A) An Alcian Blue/PAS-stained section of lung from a mouse exposed to 80 μg MWCNT and sacrificed 56 days after exposure showing a MWCNT (solid arrow) protruding through the pleura with one end lodged in a structure morphologically consistent with a subpleural lymphatic. The cells within and around the subpleural lymphatics are plasma cells. Alcian Blue/PAS stain. Bar is 10 μm. (B) Indirect immunofluorescence from the same mouse in Panel A showing staining for podoplanin, a marker of lymphatic endothelium and alveolar type I cells, in red. E-cadherin and IgG stain in green. The subpleural lymphatic (solid arrows) is revealed by the presence of podoplanin and the absence of e-cadherin, alveolar type 1 cells stain orange due to co-expression of e-cadherin and podoplanin, and plasma cells stain brilliant green due cytoplasmic to IgG (dashed arrows). (C) Indirect immunofluorescence for podoplanin demonstrates dilation of the subpleural and interstitial lymphatics (arrows) in another mouse exposed to 80 μg MWCNT and sacrificed 56 days after exposure.

actually more inflammatory than aspiration exposure, suggesting that inflammation triggered by CNT is not the result of the bolus exposure (Shvedova et al., 2008). Since failure to eliminate an inciting agent is a classic cause of chronic inflammation (Ackermann, 2007), the persistence of MWCNT within the lung and the presence of numerous macrophages containing large numbers of MWCNT suggests that in the current study, failure to eliminate the inciting cause, the MWCNT, is the cause of the persistent inflammation.

Like SWCNT exposure (Shvedova et al., 2005), MWCNT caused the very early development of fibrosis in the lung. This is a concern because lung fibrosis is an important feature of the occupational pneumoconioses caused by silica, coal dust, and asbestos (Castranova and Vallyathan, 2000; Mossman and Churg, 1998) Indeed, asbestosis, the pneumoconiosis caused by asbestos inhalation is a frequent cause of death in asbestos-exposed workers (Harding et al., 2009).

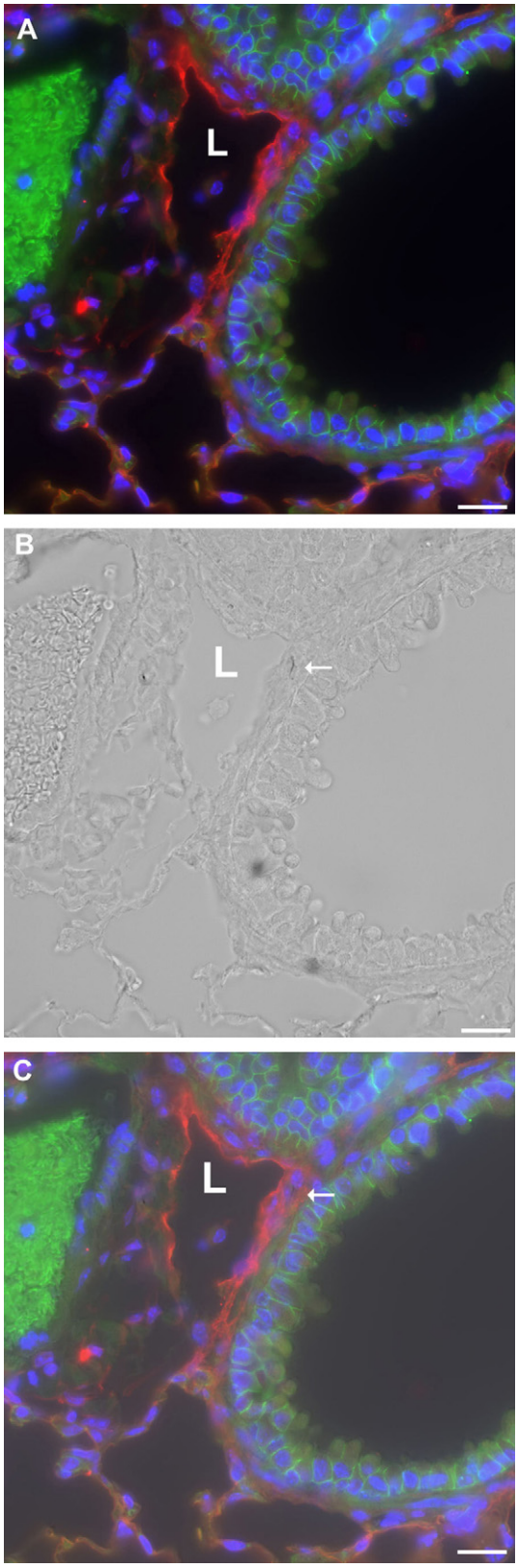

Fig. 14. Dilation of the lymphatics adjacent to bronchioles in a mouse 56 days after aspirating 80 μg MWCNT. (A) Indirect immunofluorescence for podoplanin and e-cadherin demonstrates the dilation of a peribronchiolar lymphatic (L) by the brilliant red fluorescence of its lining endothelium. (B) The same section as in A but viewed with transmitted light, demonstrating a MWCNT in lymphatic wall (arrow). (C) The superimposed images of A and B confirming the localization of the MWCNT within the lymphatic wall.

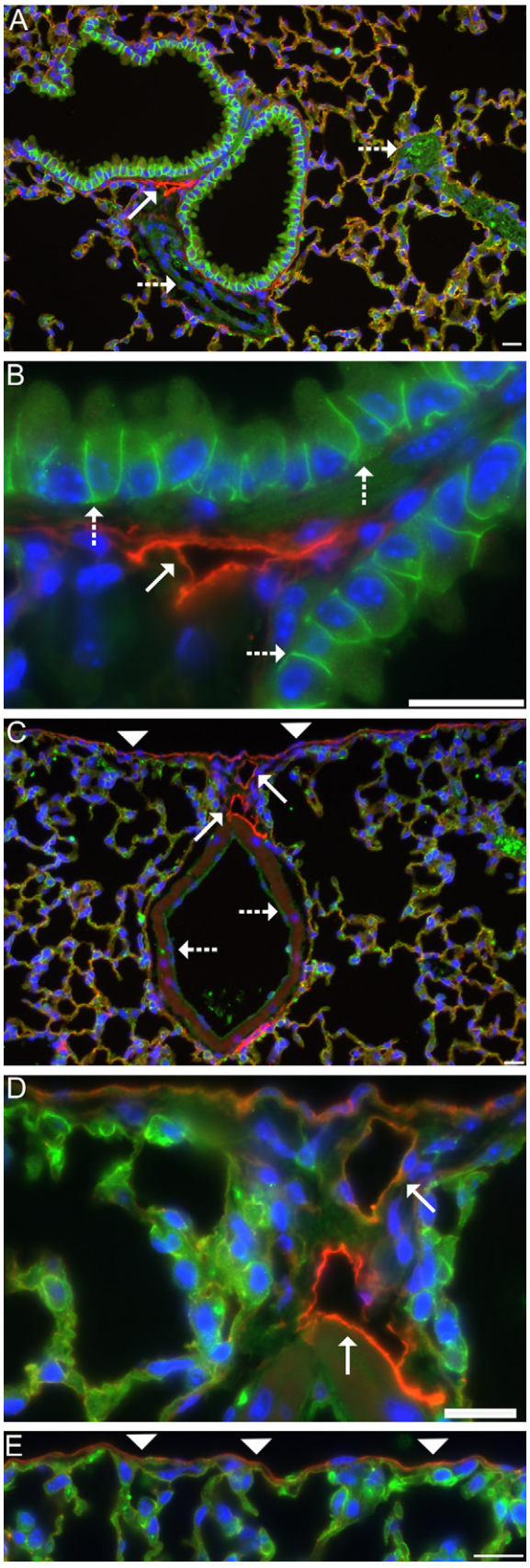

Fig. 15. Lymphatics in the lungs of control mice visualized with indirect immunofluorescence for podoplanin and e-cadherin. (A) Indirect immunofluorescence for podoplanin distinguishes lymphatic from vascular endothelium. The endothelium of the periobronchiolar lymphatics (solid arrow) is red but the vascular endothelium (dashed arrows) does not stain. (B) A higher magnification of podoplanin staining (red) in the peribronchiolar lymphatic (solid arrow). E-cadherin immunofluorescence (green) clearly demonstrates the bronchiolar epithelium (dashed arrows). (C) The lymphatic endothelium in interlobular septa (solid arrows) contains podoplanin (red) but the vascular endothelium (dashed arrows) does not. The mesothelium of the pleura (arrowheads) stains variably with podoplanin. (D) A higher magnification of interlobular lymphatics (solid arrows). (E) Red podoplanin immunofluorescence is present in the control mouse pleura (arrowheads) but no lymphatic lumen is seen. Bar is 20 μm.

An additional important finding in this study is that chronic MWCNT exposure causes lymphangiectasia, dilation of the pulmonary lymphatics. Since there was no lymphangiectasia in the controls, the lymphangiectasia was secondary lymphangiectasia, not congenital lymphangiectasia. Secondary lymphangiectasia is caused by impaired lymphatic drainage and/or increase lymph production (Faul et al., 2000). The major route for particle and fiber clearance in the lung is via the lymphatics (Harmsen et al., 1987, 1985; Trosic et al., 2000). Indeed, our observation of macrophages with large numbers of MWCNTs which sometimes protrude from their cytoplasmic membranes and the presence of MWCNTs within lymphatics walls, provides a potential explanation for impaired lymphatic drainage in the MWCNT-exposed lung. The enlarged and irregularly shaped macrophages could well have difficulty moving along the lymphatics, particularly if the lymphatic wall is inflamed due to intramural MWCNT, which were also observed in this study. Indeed, an initial delay in lymphatic clearance followed by enhanced clearance has previously been noted in exposures containing crocidolite asbestos (Trosic et al., 2000). The podoplanin immunofluorescence procedure developed during our study, allowed us to directly visualize lymphangiectasia in the MWCNT-exposed lung.

An additional consideration is that the lymphatic endothelium serves as a homing signal for alveolar macrophages to direct them from the lung to the lymphatics and from there to the draining tracheobronchial lymph node (Johnson et al., 2006; Johnson and Jackson, 2008). Therefore, as dilation of the lymphatics expands the endothelium, that should expand the homing signals and increase macrophage homing to the lymphatics. The location of the lymphatics in the lung is also important. Pulmonary lymphatics are located around the pulmonary vasculature, around airways, in interlobular septa, in perihilar tissue, and very importantly within and below the pleura (Ohtani and Ohtani, 2008). Expansion of the subpleural lymphatics, may draw MWCNT-laden macrophages to critical sites within the lung. Consistent with lymphangiectasia facilitating macrophage homing to the pleura, pleural penetration was observed in two of the four mice at 56 days after MWCNT exposure and in one of these mice, the MWCNT protruded from the dilated lymphatic through the pleura.

In summary, the data reported here indicate that doses of MWCNT tested in our mouse model represent doses relevant to estimated human occupational exposures. Specifically, our data indicate that exposure of mice to MWCNT caused dose- and time-dependant pulmonary inflammation and damage, as assessed by BAL and histopathological methods. MWCNT exposure also caused rapid development of pulmonary fibrosis. Furthermore, data were presented that demonstrated that MWCNT can reach the pleura after pulmonary exposure. However, the significance of this observation will require further, more extensive investigations, to fully assess if pleural penetration by MWCNT results in any adverse health outcomes.

Conflicts of interest

There are no competing interests.

Acknowledgements

The authors would like to thank Mitsui & Company Ltd., for the generous donation of the MWCNTs used in this study. The authors would like to thank Mr. Ming Li and Mingjia Zhi (West Virginia University, Department of Mechanical & Aerospace Engineering) for assistance with zeta potential and XPS measurements.

References

Ackermann, M.R., 2007. Chronic inflammation and wound healing. In: Zachary, M.D.M.a.J.F. (Ed.), Pathologic Basis of Veterinary Disease. Mosby Elsevier, St. Louis, pp. 153–191.
Ago, H., Kugler, T., Cacialli, F., Salaneck, W.R., Shaffer, M.S.P., Windle, A.H., Friend, R.H., 1999. Work functions and surface functional groups of multiwall carbon nanotubes. J. Phys. Chem. B 103, 8116–8121.
Baluk, P., McDonald, D.M., 2008. Markers for microscopic imaging of lymphangiogenesis and angiogenesis. Ann. N. Y. Acad. Sci. 1131, 1–12.
Castranova, V., Vallyathan, V., 2000. Silicosis and coal workers' pneumoconiosis. Environ. Health Perspect. 108 Suppl. 4, 675–684.
Chen, P., 1999. Electronic structure and optical limiting behavior of carbon nanotubes. Phys. Rev. Lett. 82, 2548–2551.
Deng, X., Jia, G., Wang, H., Sun, H., Wang, X., Yang, S., Wang, T., Liu, Y., 2007. Translocation and fate of multi-walled carbon nanotubes in vivo. Carbon 45, 1419–1424.
Dixon, D., Herbert, R.A., Sills, R.C., Boorman, G.A., 1999. Lungs, pleura, and mediastinum. In: Maronpot, R.R., Boorman, G.A., Gaul, B.W. (Eds.), Pathology of the Mouse. Cache River Press, Vienna, IL, pp. 293–332.
Donaldson, K., Tran, C.L., 2004. An introduction to the short-term toxicology of respirable industrial fibres. Mutat. Res. 553, 5–9.
Donaldson, K., Aitken, R., Tran, L., Stone, V., Duffin, R., Forrest, G., Alexander, A., 2006. Carbon nanotubes: a review of their properties in relation to pulmonary toxicology and workplace safety. Toxicol. Sci. 92, 5–22.
Endo, M., Strano, M.S., Ajayan, P.M., 2008. Potential applications of carbon nanotubes. Carbon Nanotubes 111, 13–61.
Epler, G.R., Colby, T.V., McLoud, T.C., Carrington, C.B., Gaensler, E.A., 1985. Bronchiolitis obliterans organizing pneumonia. N. Engl. J. Med. 312, 152–158.
Epler, G.R., 1992. Bronchiolitis obliterans organizing pneumonia: definition and clinical features. Chest 102, 2S–6S.
Epler, G.R., 2001. Bronchiolitis obliterans organizing pneumonia. Arch. Intern. Med. 161, 158–164.
Faul, J.L., Berry, G.J., Colby, T.V., Ruoss, S.J., Walter, M.B., Rosen, G.D., Raffin, T.A., 2000. Thoracic lymphangiomas, lymphangiectasis, lymphangiomatosis, and lymphatic dysplasia syndrome. Am. J. Respir. Crit. Care Med. 161, 1037–1046.
Felten, A., Bittencourt, C., Pireaux, J.J., 2006. Gold clusters on oxygen plasma functionalized carbon nanotubes: XPS and TEM studies. Nanotechnology 17, 1954–1959.
Fenoglio, I., Tomatis, M., et al., 2006. Reactivity of carbon nanotubes: free radical generation or scavenging activity? Free Radic. Biol. Med. 40 (7), 1227–1233.
Galer, D.M., Leung, H.W., Sussman, R.G., Trzos, R.J., 1992. Scientific and practical considerations for the development of occupational exposure limits (OELs) for chemical substances. Regul. Toxicol. Pharmacol. 15, 291–306.
Han, J.H., Lee, E.J., Lee, J.H., So, K.P., Lee, Y.H., Bae, G.N., Lee, S.B., Ji, J.H., Cho, M.H., Yu, I.J., 2008. Monitoring multiwalled carbon nanotube exposure in carbon nanotube research facility. Inhal. Toxicol. 20, 741–749.
Harmsen, A.G., Muggenburg, B.A., Snipes, M.B., Bice, D.E., 1985. The role of macrophages in particle translocation from lungs to lymph nodes. Science 230, 1277–1280.
Harmsen, A.G., Mason, M.J., Muggenburg, B.A., Gillett, N.A., Jarpe, M.A., Bice, D.E., 1987. Migration of neutrophils from lung to tracheobronchial lymph node. J. Leukoc. Biol. 41, 95–103.
Harding, A.H., Darnton, A., Wegerdt, J., McElvenny, D., 2009. Mortality among British asbestos workers undergoing regular medical examinations (1971-2005). Occup. Environ. Med. 66 (7), 487–495.
Henderson, R.F., Benson, J.M., Hahn, F.F., Hobbs, C.H., Jones, R.K., Mauderly, J.L., McClellan, R.O., Pickrell, J.A., 1985. New approaches for the evaluation of pulmonary toxicity: bronchoalveolar lavage fluid analysis. Fundam. Appl. Toxicol. 5, 451–458.
Johnson, L.A., Clasper, S., Holt, A.P., Lalor, P.F., Baban, D., Jackson, D.G., 2006. An inflammation-induced mechanism for leukocyte transmigration across lymphatic vessel endothelium. J. Exp. Med. 203, 2763–2777.
Johnson, L.A., Jackson, D.G., 2008. Cell traffic and the lymphatic endothelium. Ann. N. Y. Acad. Sci. 1131, 119–133.
Lison, D., Muller, J., 2008. To the Editor. Toxicol. Sci. 101, 179–180.
Littell, R.C., Milliken, G.A., Stroup, W.W., Wolfinger, R.D., 1996. SAS System for Mixed Models. SAS Institute Inc., Cary, NC.
Maynard, A.D., Baron, P.A., Foley, M., Shvedova, A.A., Kisin, E.R., Castranova, V., 2004. Exposure to carbon nanotube material: aerosol release during the handling of unrefined single-walled carbon nanotube material. J. Toxicol. Environ. Health A 67, 87–107.
McDonald, J., Mitchell, L., 2008. To the Editor. Toxicol. Sci. 101, 181–182.
Mercer, R.R., Scabilloni, J., Wang, L., Kisin, E., Murray, A.R., Schwegler-Berry, D., Shvedova, A.A., Castranova, V., 2008. Alteration of deposition pattern and pulmonary response as a result of improved dispersion of aspirated single-walled carbon nanotubes in a mouse model. Am. J. Physiol. Lung Cell. Mol. Physiol. 294 (1), L87–L97.
Mitchell, L.A., Gao, J., Wal, R.V., Gigliotti, A., Burchiel, S.W., McDonald, J.D., 2007. Pulmonary and systemic immune response to inhaled multiwalled carbon nanotubes. Toxicol. Sci. 100, 203–214.
Morrow, P.E., 1972. Lymphatic drainage of the lung in dust clearance. Ann. N. Y. Acad. Sci. 200, 46–65.
Mossman, B.T., Churg, A., 1998. Mechanisms in the pathogenesis of asbestosis and silicosis. Am. J. Respir. Crit. Care Med. 157, 1666–1680.
Muller, J., Huaux, F., Moreau, N., Misson, P., Heilier, J.F., Delos, M., Arras, M., Fonseca, A., Nagy, J.B., Lison, D., 2005. Respiratory toxicity of multi-wall carbon nanotubes. Toxicol. Appl. Pharmacol. 207, 221–231.
NIOSH. NIOSH Method 7300 Elements by ICP (nitric/perchloric acid ashing).
Oberdorster, G., Maynard, A., Donaldson, K., Castranova, V., Fitzpatrick, J., Ausman, K., Carter, J., Karn, B., Kreyling, W., Lai, D., Olin, S., Monteiro-Riviere, N., Warheit, D., Yang, H., Group, A.r.f.t.I.R.F.R.S.I.N.T.S.W., 2005. Principles for characterizing the potential human health effects from exposure to nanomaterials: elements of a screening strategy. Part. Fibre Toxicol. 2, 8.
Ohtani, O., Ohtani, Y., 2008. Organization and developmental aspects of lymphatic vessels. Arch. Histol. Cytol. 71, 1–22.
Pulskamp, K., Diabaté, S., et al., 2007. Carbon nanotubes show no sign of acute toxicity but induce intracellular reactive oxygen species in dependence on contaminants. Toxicol. Lett. 168 (1), 58–74.
Pinault, M, Mayne-L'Hermite, M., Reynaud, C., Pichot, V., Launois, P., Ballutaud, D., 2005. Growth of multiwalled carbon nanotubes during the initial stages of aerosol-assisted CCVD. Carbon 43, 2968–2976.
Phalen, R.F., 1984. Basic morphology and physiology of the respiratory tract. In: Inhalation Studies: Foundattions and Techniques. CRC Press, Boca Raton, pp. 33–75.
Porter, D.W., Hubbs, A.F., Baron, P.A., Millecchia, L.L., Wolfarth, M.G., Battelli, L.A., Schwegler-Berry, D.E., Beighley, C.M., Andrew, M.E., Castranova, V., 2007. Pulmonary toxicity of expancel microspheres in the rat. Toxicol. Pathol. 35, 702–714.
Porter, D., Sriram, K., Wolfarth, M., Jefferson, A., Schwegler-Berry, D., Andrew, M.E., Castranova, V., 2008. A biocompatible medium for nanoparticle dispersion. Nanotoxicology 2, 144–154.
Porter, D.W., Wolfarth, M.G., Chen, B.T., McKinney, W., Hubbs, A.F., Battelli, L., Andrew, A., Frazier, D.G., Castranova, V., 2009. Pulmonary toxicity of inhaled multi-walled carbon nanotubes. Toxicologist 108, 457.
Ryu, J.H., Myers, J.L., Swensen, S.J., 2003. Bronchiolar disorders. Am. J. Respir. Crit. Care Med. 168, 1277–1292.
Shvedova, A.A., Kisin, E.R., Mercer, R., Murray, A.R., Johnson, V.J., Potapovich, A.I., Tyurina, Y.Y., Gorelik, O., Arepalli, S., Schwegler-Berry, D., Hubbs, A.F., Antonini, J., Evans, D.E., Ku, B.K., Ramsey, D., Maynard, A., Kagan, V.E., Castranova, V., Baron, P., 2005. Unusual inflammatory and fibrogenic pulmonary responses to single-walled carbon nanotubes in mice. Am. J. Physiol. Lung Cell. Mol. Physiol. 289, L698–L708.
Shvedova, A.A., Kisin, E., Murray, A.R., Johnson, V.J., Gorelik, O., Arepalli, S., Hubbs, A.F., Mercer, R.R., Keohavong, P., Sussman, N., Jin, J., Yin, J., Stone, S., Chen, B.T., Deye, G., Maynard, A., Castranova, V., Baron, P.A., Kagan, V.E., 2008. Inhalation vs. aspiration of single-walled carbon nanotubes in C57BL/6 mice: inflammation, fibrosis, oxidative stress, and mutagenesis. Am. J. Physiol. Lung Cell. Mol. Physiol. 295, L552–L565.
Stankovich, S., 2006. Stable aqueous dispersions of graphitic nanoplatelets via the reduction of exfoliated graphite oxide in the presence of poly(sodium 4-styrenesulfonate). J. Mater. Chem. 16, 155–158.
Stone, K.C., Mercer, R.R., Gehr, P., Stockstill, B., Crapo, J.D., 1992. Allometric relationships of cell numbers and size in the mammalian lung. Am. J. Respir. Cell Mol. Biol. 6, 235–243.
Tenne, R., Remskar, M., Enyashin, A., Seifert, G., 2008. Inorganic nanotubes and fullerene-like structures (IF). Carbon Nanotubes 111, 631–671.
Trosic, I., Matausic-Pisl, M., Hors, N., 2000. Pathways and quantification of insoluble particles in the lung compartments of the rat. Int. J. Hyg. Environ. Health 203, 39–43.
Warheit, D.B., Laurence, B.R., Reed, K.L., Roach, D.H., Reynolds, G.A., Webb, T.R., 2004. Comparative pulmonary toxicity assessment of single-wall carbon nanotubes in rats. Toxicol. Sci. 77, 117–125.
Warheit, D.B., 2008. How meaningful are the results of nanotoxicity studies in the absence of adequate material characterization? Toxicol. Sci. 101, 183–185.
Williams, G.T., Williams, W.J., 1983. Granulomatous inflammation—a review. J. Clin. Pathol. 36, 723–733.